Article:
Zhang, F, Liu, T, Huo, Y et al. (2 more authors) (2017) Investigation of the operating conditions to morphology evolution of β-l-glutamic acid during seeded cooling crystallization. Journal of Crystal Growth, 469. pp. 136-143. ISSN 0022-0248

https://doi.org/10.1016/j.jcrysgro.2016.09.041

Investigation of the operating conditions to morphology evolution of β-L-glutamic acid during seeded cooling crystallization

Fangkun Zhang[a], Tao Liu [a, *], Yan Huo[a], Runduo Guan[a], Xue Z. Wang[b, c]

[a]Institute of Advanced Control Technology, Dalian University of Technology, Dalian, 116024, P. R. China
[b]Institute of Particle Science and Engineering, School of Chemical and Process Engineering, University of Leeds, Leeds LS2 9JT, UK
[c] School of Chemistry and Chemical Engineering, South China University of Technology, Guangzhou 510640, China
* Corresponding author. E-mail: tliu@dlut.edu.cn; Tel: +86-411-84706465 Fax: +86-411-84706706

Abstract: In this paper the effects of operating conditions including cooling rate, initial supersaturation, and seeding temperature were investigated on the morphology evolution of β-L-glutamic acid (β-LGA) during seeded cooling crystallization. Based on the results of in-situ image acquisition of the crystal morphology evolution during the crystallization process, it was found that the crystal products tend to be plate-like or short rod-like under a slow cooling rate, low initial supersaturation, and low seeding temperature. In the opposite, the operating conditions of a faster cooling rate, higher initial supersaturation, and higher seeding temperature tend to produce long rod-like or needle-like crystals, and meanwhile, the length and width of crystal products will be increased together with a wider crystal size distribution (CSD). The aspect ratio of crystals, defined by the crystal length over width measured from in-situ or sample images, was taken as a shape index to analyze the crystal morphologies. Based on comparative analysis of the experimental results, guidelines on these operating conditions were given for obtaining the desired crystal shapes, along with the strategies for obtaining a narrower CSD for better product quality. Experimental verifications were performed to illustrate the proposed guidelines on the operating conditions for seeded cooling crystallization of LGA solution.

Keywords: Seeded cooling crystallization, morphology evolution, L-Glutamic acid, operating conditions, crystal shape, aspect ratio

---

1. Introduction

Crystal morphology relating to crystal habit or shape is critical for the end-use product quality and efficacy (e.g. bioavailability for pharmaceuticals), and affects the flowability and filtrability of down-stream processing in engineering applications. Due to the fact that it was not easy to measure the crystal shapes during a crystallization process, evaluation of crystal morphology evolution during crystallization had been mainly simplified as estimating the one-dimensional crystal size distribution (CSD) in the literature [1]. With the development of real-time process analytical technology (PAT) in the recent years, on-line measurement of crystal morphology has become available and attracted increasing attentions to study the dynamic evolution of crystal population during crystallization [1, 2].

L-glutamic acid (LGA) is a class of amino acid widely used in pharmaceutical and food industries, which mainly includes two polymorphs [3]: metastable α form and stable β form. The stable β-LGA crystal morphology was primarily described as needle-like or rod-like form in the existing references (e.g. [4, 5]). However, little attention was devoted to the LGA shape evolution in a seeded crystallization process. In fact, it has been recognized that the β-LGA crystals have a few different morphologies, e.g. needle-like [3], rod-like [6], lozenge-like [7], and plate-like [8], as shown in Figure 1. Owing to that the needle-like shape crystal has a relatively fast growth rate in the length direction, analysis of CSD for β-LGA crystals was simplified to the estimation of one-dimensional distribution, i.e. the length distribution, while the width distribution was neglected [9, 10]. It has been recognized that the needle-like crystals with a high-aspect-ratio of length over width bring difficulties to down-stream processing, thus undesirable for industrial applications. Previous works had been mainly devoted to one-dimensional CSD analysis and shape control [1, 11]. Calderon et al. presented a multi-scale image analysis method for monitoring the real-time shape evolution of LGA crystals [11]. Huo et al. developed a synthetic image analysis strategy for in-situ crystal shape identification [12]. Based on using a noninvasive stereoscopic image acquisition system, multidimensional population crystal morphology analysis was explored in terms of image processing methods [13, 14]. The influence of amino acid additives on the LGA crystal morphologies was investigated in the references [15, 16]. Shaikh et

al. simulated the crystal shape evolution using a polyhedral population balance model (PBM) [17]. For the control of LGA crystal shape during a crystallization process, closed-loop feedback control strategies [18, 19] were developed based on measurement of supersaturation and temperature.

However, little analysis had been devoted to the impact of operating conditions on β-LGA crystal morphology, e.g. the cooling rate, seeding temperature, and initial supersaturation. In fact, these operating conditions have important effect on the physical properties and quality of final products. Ni et al. [20, 21] qualitatively investigated the effects of seeding, cooling rate, material of baffles, final temperature and solution concentration on the LGA polymorph during crystallization, respectively. Tahri et al. [7] stressed the effect of solution agitation together with the temperature and supersaturation level on the LGA polymorph by cooling crystallization. The potential influence of the cooling rate and the seeding temperature on the supersaturation profile and the evolution of CSD was discussed in the literature [22]. Beck et al. [23] found that the effect of initial supersaturation and temperature basically determines the polycrystalline (or spherulitic) growth of LGA and aromatic amine. Jiang et al. [24] explored a temperature cycling strategy to modify the crystal shape of monosodium glutamate (MSG), effectively improving the CSD of final products. The dependence on initial supersaturation for producing the desired crystal morphology was investigated in and Parimaladevi and Srinivasan [25] for spontaneous crystallization of alpha-lactose monohydrate crystals.

To make clear the potential effects of different operating conditions on the β-LGA crystal shape evolution, this paper investigated the main operating conditions for seeded cooling crystallization of LGA, including the cooling rate, seeding temperature, and initial supersaturation. Experiments of different combinations on these operating conditions were conducted to study the β-LGA morphology evolution during the seeded cooling crystallization. Accordingly, some guidelines were summarized for obtaining the desired crystal shape in end-products.

2. Experiments

2.1 Material and experimental set-up

The β form LGA crystals (produced by Sigma) with a purity of at least 99% were taken as the solute, and the distilled water was used as the solution in this study.

The experimental set-up is shown in Figure 2, consisting of a 1 L jacketed glass crystallizer, a thermostatic circulator (Julabo-CF41), a Pt100 temperature probe and a PTFE four-paddle Agitator. The ATR-FTIR spectroscopy with ReactIR15 software (made by Mettler-Toledo) was used to collect the absorbance spectra of LGA solution for concentration prediction. An in-situ noninvasive stereo imaging system with two high-resolution cameras (made by Pharmavision) was used to monitor the crystal shape evolution during crystallization. The cameras (UI-2280SE-C-HQ) with CCD sensors and USB Video Class standard were made by IDS Imaging Development Systems GmbH, which is able to take maximum 6.5 images per second with the pixel resolution of 2448×2050. An off-line confocal microscope (Leica DM2500) was used to check the crystal shape information of end-products.

2.2 Seed preparation

To prepare the seeding for cooling crystallization, the β-LGA crystal seeds (produced by Sigma) were first milled, sieved, and washed by water. Then the wet crystals were put into slightly unsaturated aqueous solution under stirring for one hour, so as to polish the crystal surfaces and dissolve the fines. Subsequently, the crystals were taken out from the aqueous solution, dried, and sieved to obtain the specific size range (58-106 μm) for experiment. Figure 3 shows a snapshot of the seeds and the corresponding shape density distribution used for experiment, by using the above noninvasive imaging system when these seeds were suspended in the solution. By observing 2279 particles among the crystal seeds using the above imaging system, it was verified that the shape density distribution of these seeds is approximately the bivariate normal distribution, with the mean values of 83.0 μm and 48.1 μm and the corresponding variances of 33.8 and 17.0 for the length and width, respectively. Note that the image analysis method developed in our recent paper [13] was adopted to measure the crystal

lengths and widths, which was based on the best-fit rectangle method [26] for each crystal shape. Correspondingly, the aspect ratio used to describe the crystal shape in the references [27, 28] is herein taken as a shape index, which is defined by

$$a = L/W \tag{1.1}$$

where a denotes the crystal aspect ratio, L the measured length (μm) and W the measured width (μm) for each crystal.

The average aspect ratio for the above observed particles was computed as 1.73 based on the above definition. Assuming that all the seeds have the same shape distribution as the above observation, the shape density distribution for all the seeds was then deduced from the corresponding weights among these seeds. Moreover, the same measurement method was made for end-products by the cooling crystallization.

2.3 Experimental tests

The 1 L jacketed glass crystallizer with 500 ml distilled water was first heated up to about 75 °C and stirred at a constant speed of 200 rpm. Then, the prepared β-form LGA crystals were put into the crystallizer for about 120 min at 75 °C under the constant stirring, so as to guarantee complete dissolution. Subsequently, the solution was cooled down at a speed of 1 °C/min to the seeding temperature, e.g. 45 °C. According to the β-LGA solubility equation given in the reference [29], the solubility is estimated by

$$\begin{aligned} c_{\beta}^{*} = {} & 2.204 - 7.322\times10^{-2}\times T + 8.93\times10^{-3}\times T^{2} \\ & -1.48183\times10^{-4}\times T^{3} + 1.34069\times10^{-6}\times T^{4} \end{aligned} \tag{1.2}$$

$$S = \frac{c}{c_{\beta}^{*}} \tag{1.3}$$

where c_{β}^{*} is the solubility of β-LGA in g/L, T the solution temperature in Celsius, S the supersaturation ratio, and c the solution concentration. For seeding, additional 2% β-LGA crystal seeds are used to add in the supersaturated solution.

Based on the above initial preparation, different operating conditions including cooling rate, seeding temperature and initial supersaturation are conducted for batch cooling crystallization, as listed in Table 1. Three different cooling rates, slow (0.05 °C/min), moderate (0.1 °C/min), and

fast (0.2 °C/min), were carried out for comparison, while the seeding temperature and initial supersaturation were maintained constant, i.e. 45 °C and 1.2, respectively. The tests on initial supersaturation were performed by changing it from a relatively low value of 1.1 to the maximum of 1.3, while the cooling rate and seeding temperature were maintained constant as in the cases of B1 and B2 shown in Table 1, so as to make comparison with A2. In addition, the tests on seeding temperature were investigated in the cases of C1 and C2 shown in Table 1, which can also be compared with A3.

It should be noted that the cooling rate and the initial supersaturation should not be taken much faster or higher. Otherwise, undesired secondary nucleation will be provoked, leading to crystal agglomeration and a mass of fines. For example, it can be easily verified that taking the initial supersaturation of 1.3 with a cooling rate of 0.2 °C/min and a seeding temperature of 55 °C for crystallization would result in bimodal product distribution accompanied with a significant account of fines. Besides, the higher the seeding temperature, the narrower the operating range of initial supersaturation.

All the above experiments were performed for the same duration of 90 minutes for comparison, with the above noninvasive imaging acquisition system for monitoring the crystal morphology evolution. A scenario of product snapshot captured by the above imaging system was shown in Figure 4. The crystal shape distribution was counted by using the in-situ image analysis method developed in our recent paper [12]. At the end of each crystallization experiment, the crystal products were sampled from the crystallizer, and then filtered and dried for off-line analysis using the confocal microscope.

3. Results and discussions

Table 2 lists the experimental results based on measuring the lengths and widths of over 2000 samples from each test. It is obviously seen from the means of crystal length and width and the averaged aspect ratios that there is a common trend on the crystal size and shape by manipulating the cooling rate, seeding temperature, and initial supersaturation, i.e. the crystal length and aspect ratio are monotonically increased by taking higher values of cooling rate,

seeding temperature, and initial supersaturation, and vice versa. Further analysis on the crystal shape evolution is detailed below.

(1) Crystal shape

The offline microscopy images of crystal products by using different operating conditions are shown in Figure 5. It is seen that the produced crystals are inclined to be the plate-like shape under the operating conditions of B1 and C1, or short rod-like shape under the operating conditions of A1 and A2. In contrast, long rod-like crystals with a higher aspect ratio were obtained under the operating conditions of A3, B2 and C2. By comparing the results listed in Table 2 under the operating conditions of A1, A2, A3, it is found that a slower cooling rate yields short rod-like crystals with a lower aspect ratio, with respect to the moderate seeding temperature (i.e. 45 °C) and initial supersaturation (i.e. 1.2). Comparing the results under the operating conditions of B1 and B2, it is seen that a lower initial supersaturation yields plate-like crystals with a lower aspect ratio, with respect to the moderate cooling rate (i.e. 0.1 °C/min) and seeding temperature (i.e. 45 °C). Comparing the results under the operating conditions of C1 and C2, it is seen that a lower seeding temperature yields plate-like or short rod-like crystals with a lower aspect ratio, with respect to the high cooling rate (i.e. 0.2 °C/min) and moderate initial supersaturation (i.e. 1.2).

The above results indicate that the desired LGA crystal shapes can be obtained by manipulating the cooling rate, seeding temperature, and initial supersaturation for cooling crystallization. Table 3 shows the increasing trend of the averaged aspect ratio with respect to the changes of the cooling rate (see A1, A2, A3) and the seeding temperature (see C1, A3, C2), respectively, in terms of the same initial supersaturation (i.e. 1.2). In contrast, Table 4 shows the increasing trend of the averaged aspect ratio with respect to the changes of the cooling rate (see A1, A2, A3) and initial supersaturation (see B1, A2, B2), respectively, in terms of the same seeding temperature (i.e. 45 °C).

In addition, it can be seen from Table 3 that the crystal products had a relatively low aspect ratio of 2.45 under the seeding temperature of 35 °C. In contrast, relatively high aspect ratios (4.05 and 4.31) were obtained under the seeding temperatures of 45 °C and 55 °C, respectively,

based on the same cooling rate (0.2 °C/min) and initial supersaturation (1.2). This indicates that given the cooling rate and initial supersaturation for cooling crystallization, a lower seeding temperature facilitates yielding plate-like or short rod-like crystals.

Based on the above analysis, some guidelines on the operating conditions for obtaining the plate-like, rod-like, or needle-like crystals are given below:

(a) Taking the cooling rate slower than 0.2 °C/min, the seeding temperature below 45 °C combined with the initial supersaturation lower than 1.1, or the seeding temperature below 35 °C combined with the initial supersaturation lower than 1.2, the crystal products tend to be plate-like or short rod-like, with an averaged aspect ratio smaller than 2.45. Moreover, taking a lower seeding temperature yields more plate-like crystal products with a lower averaged aspect ratio;

(b) Taking the cooling rate no slower than 0.2 °C/min, the seeding temperature no lower than 45 °C, and the initial supersaturation no lower than 1.2, the crystal products tend to be long rod-like or needle-like, with an averaged aspect ratio higher than 4.05. Moreover, taking a lower seeding temperature towards 45 °C yields more rod-like crystal products with a lower averaged aspect ratio.

(2) CSD and crystal shape distribution (CShD)

CSD has been mainly used to characterize the crystal products in industry, based on one-dimensional measurement or estimation of crystal size or shape. Little result, however, had been cultivated for the CShD related to crystal aspect ratio during crystallization, due to the limitation of measurement and available PATs. With the development of on-line imaging systems for real-time monitoring of crystallization processes, it has become possible to measure the shapes of particles during a crystallization process, and therefore increasing efforts have been devoted to the crystal shape control in the recent years [1, 2].

Figure 6 shows the CShDs under different operating conditions, based on using the in-situ imaging analysis method [13]. Comparing the results shown in Figure 6(a) under the operating conditions of A1, A2, A3, it is found that a faster cooling rate increases the length and width of

crystal products, and widens the range of CShD while the density ($F(x)$) center is moved towards an area of higher aspect ratio, which is in coherence with the changes of crystal length and width together with the variances listed in Table 2. Similar conclusions can be drawn from Figure 6(b) and (c) for comparing the results of changing the initial supersaturation (see B1 and B2), or the seeding temperature (see C1 and C2), respectively. A general guideline for expediting the crystal growth is therefore given as taking a relatively faster cooling rate, or a relatively higher initial supersaturation, or a relatively higher seeding temperature to increase the length and width of crystal products, when the remaining operating conditions are prescribed.

Figure 7 shows the CSD of crystal products in length under seven different operating conditions. It is seen that the length distributions of A3, B2 and C2 are wider than those of A1, B1 and C1. This is because faster crystal growth were obtained under the operating conditions of A3, B2 and C2. In other words, a narrower CSD can be produced by taking a slower cooling rate, or a lower initial supersaturation, or a lower seeding temperature, and vice versa. Hence, in order to obtain a narrow CSD, a guideline is to take a relative slower cooling rate, or a relative lower initial supersaturation, or a lower seeding temperature for crystallization, when the remaining operating conditions are prescribed. However, one disadvantage is that the crystal growth rate will become slower by taking such operating condition, thus at the cost of longer time to obtain larger crystals. For example, the crystal mean length of B1 is 149.6 μm with the initial supersaturation taken as 1.1, almost only a half of the crystal mean length of B2 (238.5 μm) with the initial supersaturation taken as 1.3.

In addition, it was found by the experimental study that the LGA product shape and quality are closely related to the seeds quality, including the seed size, shape, and surface smoothness. For example, shaggy seeds with coarse surfaces are inclined to provoke crystal aggregation even under a relatively low supersaturation, and therefore affect the product quality. Moreover, a narrow seed size (shape) distribution with uniformity in the seeds is necessary for obtaining larger and uniform products from a size-dependent crystal growth process like the seeded cooling crystallization.

4. Experimental verification

To verify the above conclusions and guidelines for seeded cooling crystallization, two experiments were carried out with the operating conditions listed in Table 5. The experimental set-up and seeds were the same as the previous experiments. Figure 8 shows the offline microscopy images of the crystal products. The analysis results are summarized in Table 6, along with comparisons on the averaged aspect ratios of crystal products shown in Tables 3 and 4.

It is seen from Figure 8 that plate-like crystals were obtained under the operating condition of E1 as expected, corresponding to a low average aspect ratio of 2.37 shown in Table 6. In contrast, taking the operating condition of E2 results in the expected long rod-like crystals, corresponding to a high average aspect ratio 4.68. Both of them are consistent with the above analysis results. Meanwhile, it is seen from Table 6 that smaller variances of the crystal length and width were obtained under E1, corresponding to a flatter CShD compared to that of E2. On the other hand, E2 led to faster crystal growth compared to E1. The comparison results shown in Tables 3 and 4 well demonstrate the above conclusions and guidelines.

5. Conclusions

This paper has investigated the effects of operating conditions on β-LGA crystal shape evolution during seeded cooling crystallization, including the cooling rate, seeding temperature, and initial supersaturation. Different experiments covering the possible ranges of these operating conditions were performed for analysis, respectively. It was found that the crystal products tend to be plate-like or short rod-like under a slow cooling rate, low initial supersaturation, and low seeding temperature. In the opposite, the operating conditions of a faster cooling rate, higher initial supersaturation, and higher seeding temperature tend to produce long rod-like or needle-like crystals. Guidelines on these operating conditions has been given for obtaining the desired crystal shapes in practice. Concerning the β-LGA crystal shape evolution, it was found that a faster cooling rate, or a higher initial supersaturation, or a higher seeding temperature increases the length and width of crystal products, and widens the range of CShD while the density center is moved towards an area of higher aspect ratio. Guidelines are therefore given for

how to expedite the crystal growth in the length and width, or slow down the crystal growth to obtain a narrower CSD for better product quality. Experimental verifications have well demonstrated the proposed guidelines on the operating conditions for obtaining the expected crystal shapes in end-products in terms of the seeded cooling crystallization of LGA solution.

Acknowledgement

This work is supported in part by the National Thousand Talents Program of China, NSF China Grants 61473054, 61633006, and 21306017, and the Fundamental Research Funds for the Central Universities of China. We would like to thank Dr. Cai Y. Ma for valuable discussions and support.

References

[1] Z.K. Nagy, R.D. Braatz, Advances and new directions in crystallization control, Annual Review of Chemical and Biomolecular Engineering, 3 (2012) 55-75.

[2] C.Y. Ma, J.J. Liu, X.Z. Wang, Measurement, modelling, and closed-loop control of crystal shape distribution: Literature review and future perspectives, Particuology, 26 (2016) 1-18.

[3] M. Kitamura, Polymorphism in the crystallization of L-glutamic acid, Journal of Crystal Growth, 96 (1989) 541-546.

[4] A. Borissova, S. Khan, T. Mahmud, K.J. Roberts, J. Andrews, P. Dallin, Z.P. Chen, J. Morris, In situ measurement of solution concentration during the batch cooling crystallization of L-glutamic acid using ATR-FTIR spectroscopy coupled with chemometrics, Crystal Growth & Design, 9 (2009) 692-706.

[5] R. Beck, A. Häkkinen, D. Malthe-Sørenssen, J.-P. Andreassen, The effect of crystallization conditions, crystal morphology and size on pressure filtration of L-glutamic acid and an aromatic amine, Separation and Purification Technology, 66 (2009) 549-558.

[6] C.Y. Ma, X.Z. Wang, K.J. Roberts, Multi-dimensional population balance modeling of the growth of rod-like L-glutamic acid crystals using growth rates estimated from in-process imaging, Advanced Powder Technology, 18 (2007) 707-723.

[7] Y. Tahri, E. Gagnière, E. Chabanon, T. Bounahmidi, D. Mangin, Investigation of the l-Glutamic acid polymorphism: Comparison between stirred and stagnant conditions, Journal of Crystal Growth, 435 (2016) 98-104.

[8] C. Cashell, D. Corcoran, B.K. Hodnett, Secondary nucleation of the β-polymorph of L-glutamic acid on the surface of α-form crystals, Chemical Communications, (2003) 374-375.

[9] M. Kitamura, T. Ishizu, Growth kinetics and morphological change of polymorphs of L-glutamic acid, Journal of Crystal Growth 209 (2000) 138-145.

[10] N.E. Briggs, U. Schacht, V. Raval, T. McGlone, J. Sefcik, A.J. Florence, Seeded crystallization of β-L-glutamic acid in a continuous oscillatory baffled crystallizer, Organic Process Research & Development, 19 (2015) 1903-1911.

[11] J. Calderon De Anda, X.Z. Wang, K.J. Roberts, Multi-scale segmentation image analysis for

the in-process monitoring of particle shape with batch crystallisers, Chemical Engineering Science, 60 (2005) 1053-1065.

[12] Y. Huo, T. Liu, H. Liu, C.Y. Ma, X.Z. Wang, In-situ crystal morphology identification using imaging analysis with application to the L-glutamic acid crystallization, Chemical Engineering Science, 148 (2016) 126-139.

[13] S. Schorsch, D.R. Ochsenbein, T. Vetter, M. Morari, M. Mazzotti, High accuracy online measurement of multidimensional particle size distributions during crystallization, Chemical Engineering Science, 105 (2014) 155-168.

[14] C.Y. Ma, J.J. Liu, X.Z. Wang, Stereo imaging of crystal growth, AIChE Journal, 62 (2016) 18-25.

[15] Y. Mo, L. Dang, H. Wei, L-Glutamic acid polymorph control using amino acid additives, Industrial & Engineering Chemistry Research, 50 (2011) 10385-10392.

[16] Y. Zhang, J.J. Liu, J. Wan, X.Z. Wang, Two dimensional population balance modelling of crystal growth behaviour under the influence of impurities, Advanced Powder Technology, 26 (2015) 672-678.

[17] L.J. Shaikh, V.V. Ranade, A.B. Pandit, Crystal shape evolution using polyhedral population balance, Industrial & Engineering Chemistry Research, 53 (2014) 18966-18974.

[18] N.C.S. Kee, R.B.H. Tan, R.D. Braatz, Selective crystallization of the metastable α-Form of L-glutamic acid using concentration feedback control, Crystal Growth & Design, 9 (2009) 3044-3051.

[19] C.Y. Ma, X.Z. Wang, Closed-loop control of crystal shape in cooling crystallization of L-glutamic acid, Journal of Process Control, 22 (2012) 72-81.

[20] X. Ni, A. Liao, Effects of cooling rate and solution concentration on solution crystallization of L-glutamic acid in an oscillatory baffled crystallizer, Crystal Growth & Design, 8 (2008) 2875-2881.

[21] X. Ni, A. Liao, Effects of mixing, seeding, material of baffles and final temperature on solution crystallization of L-glutamic acid in an oscillatory baffled crystallizer, Chemical Engineering Journal, 156 (2010) 226-233.

[22] M. Oullion, F. Puel, G. Févotte, S. Righini, P. Carvin, Industrial batch crystallization of a

plate-like organic product. In situ monitoring and 2D-CSD modelling: Part 1: Experimental study, Chemical Engineering Science, 62 (2007) 820-832.

[23] R. Beck, E. Flaten, J.P. Andreassen, Influence of crystallization conditions on the growth of polycrystalline particles, Chemical Engineering & Technology, 34 (2011) 631-638.

[24] M. Jiang, X. Zhu, M.C. Molaro, M.L. Rasche, H. Zhang, K. Chadwick, D.M. Raimondo, K.-K.K. Kim, L. Zhou, Z. Zhu, M.H. Wong, D. O'Grady, D. Hebrault, J. Tedesco, R.D. Braatz, Modification of crystal shape through deep temperature cycling, Industrial & Engineering Chemistry Research, 53 (2014) 5325-5336.

[25] P. Parimaladevi, K. Srinivasan, Influence of supersaturation level on the morphology of alpha-lactose monohydrate crystals, International Dairy Journal, 39 (2014) 301-311.

[26] W. Wang, Image analysis of particles by modified Ferret method-best-fit rectangle, Powder Technology, 165 (2006) 1-10.

[27] M. Takasuga, H. Ooshima, Control of crystal aspect ratio and size by changing solvent composition in oiling out crystallization of an active pharmaceutical ingredient, Crystal Growth & Design, 15 (2015) 5834-5838.

[28] S. Kudo, Y. Suzaki, T. Hino, S. Kato, H. Takiyama, Growth and dissolution kinetics for methacrylic acid crystal in melt, Journal of Chemical Engineering of Japan, 48 (2015) 922-926.

[29] R.F. Li, X.Z. Wang, S.B. Abebe, Monitoring batch cooling crystallization using NIR: development of calibration models using genetic algorithm and PLS, Particle & Particle Systems Characterization, 25 (2008) 314-327.

Tables and Figures

Table 1. Operating conditions of batch cooling crystallization experiments

Batch No.	Cooling rate (°C/min)	Seeding temperature (°C)	Initial supersaturation
A1	0.05	45	1.2
A2	0.1	45	1.2
A3	0.2	45	1.2
B1	0.1	45	1.1
B2	0.1	45	1.3
C1	0.2	35	1.2
C2	0.2	55	1.2

Table 2. Image analysis results of crystal products under different operating conditions

Run No.	Number of sampled particles	Mean length (μm)	Mean width (μm)	Variance in length (-)	Variance in width (-)	Average aspect ratio (-)
Seed	2279	83.0	48.1	33.8	17.0	1.73
A1	2641	173.9	60.7	78.4	32.2	2.86
A2	2243	197.1	63.5	81.2	38.5	3.39
A3	2084	333.9	82.3	102.3	51.4	4.05
B1	2497	149.6	62.5	63.5	31.8	2.39
B2	2790	238.5	65.3	101.2	45.4	3.65
C1	2748	155.1	63.1	70.3	33.0	2.45
C2	2584	401.4	93.1	124.9	69.0	4.31

Table 3. Averaged aspect ratios of crystal products under the initial supersaturation level of 1.2

Cooling rate \ Seeding temperature	35°C	45°C	55°C
0.05°C/min		2.86	
0.1°C/min	2.37*	3.39	
0.2°C/min	2.45	4.05	4.31

* Experimental verification result

Table 4. Averaged aspect ratios of crystal products under the same seeding temperature 45 °C

Initial supersaturation / Cooling rate	1.1	1.2	1.3
0.05°C/min		2.86	
0.1°C/min	2.39	3.39	3.65
0.2°C/min		4.05	4.68*

* Experimental verification result

Table 5. Operating conditions of verification experiments

Run No.	Cooling rate (°C/min)	Seeding temperature (°C)	Initial supersaturation
E1	0.1	35	1.2
E2	0.2	45	1.3

Table 6. Image analysis results of verification experiments

Run No.	Number of sampled particles	Mean length (μm)	Mean width (μm)	Variance in length (-)	Variance in width (-)	Average aspect ratio (-)
E1	2012	139.2	58.7	59.1	26.9	2.37
E2	2103	395.7	84.5	118.4	65.0	4.68

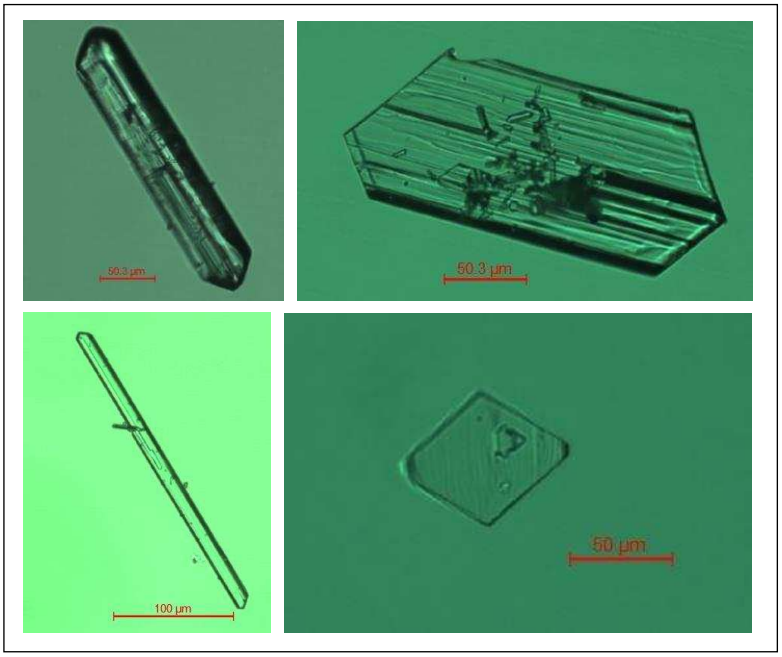

Figure 1. Different β-LGA crystal morphologies recognized in the literature: (a) rod-like; (b) plate-like; (c) needle-like; (d) lozenge-like

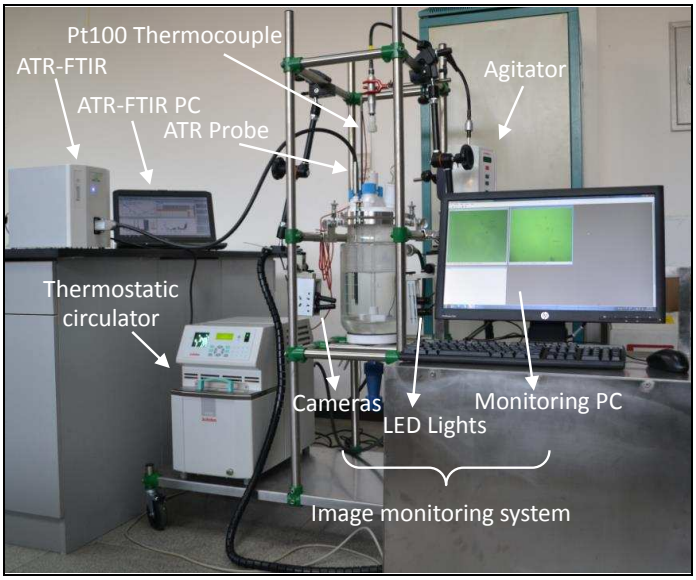

Figure 2. Experimental set-up for in-situ image monitoring of seeded cooling crystallization

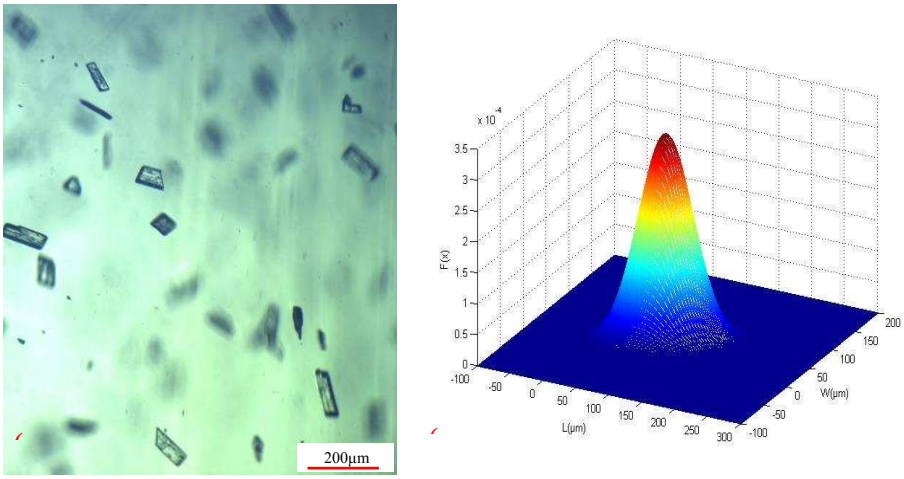

(a) **(b)**

Figure 3. (a) Snapshot of crystal seeds by an in-situ imaging system; (b) Shape density distribution of crystal seeds

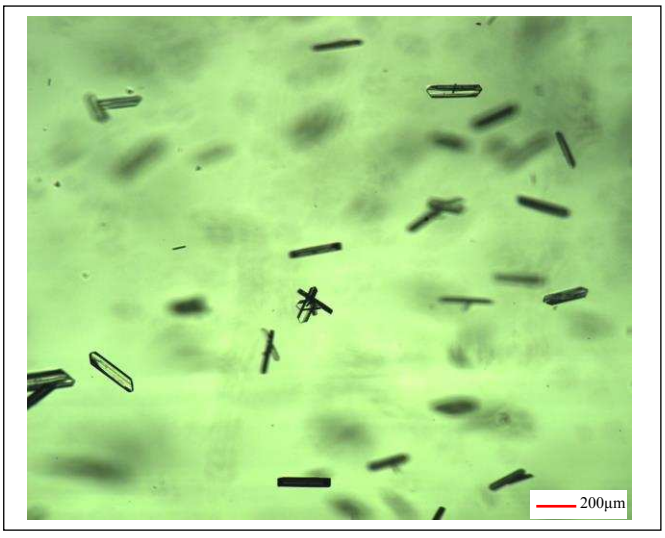

Figure 4. Snapshot of crystal products by an in-situ imaging system

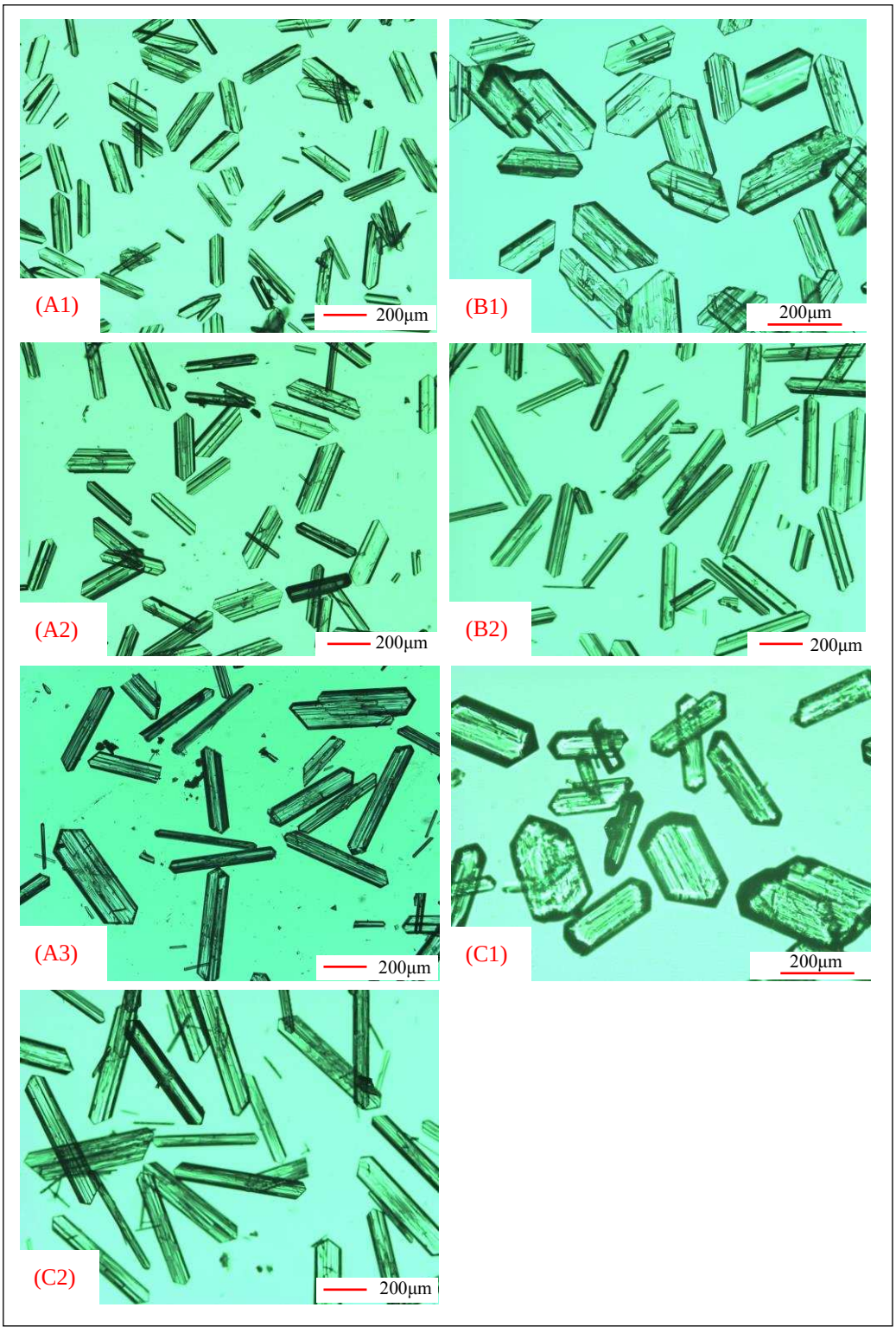

Figure 5. Microscopy images of crystal products by different operating conditions

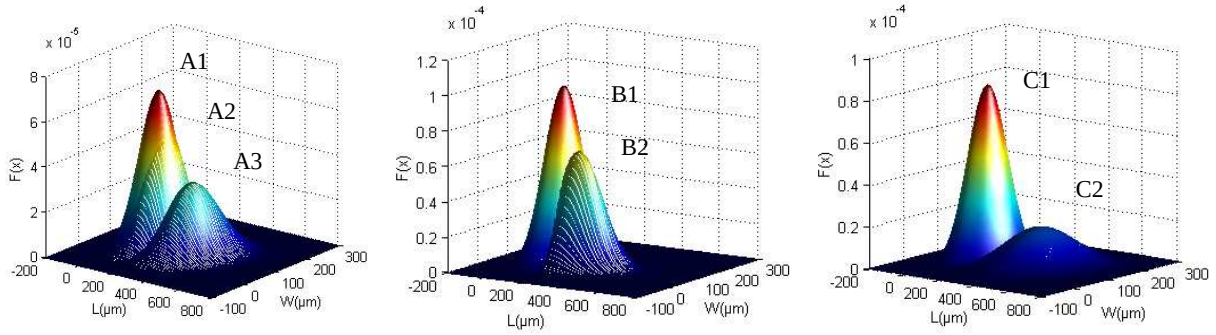

(a) **(b)** **(c)**

Figure 6. Plots of CShD under different operating conditions: (a) cooling rate; (b) initial supersaturation; (c) seeding temperature

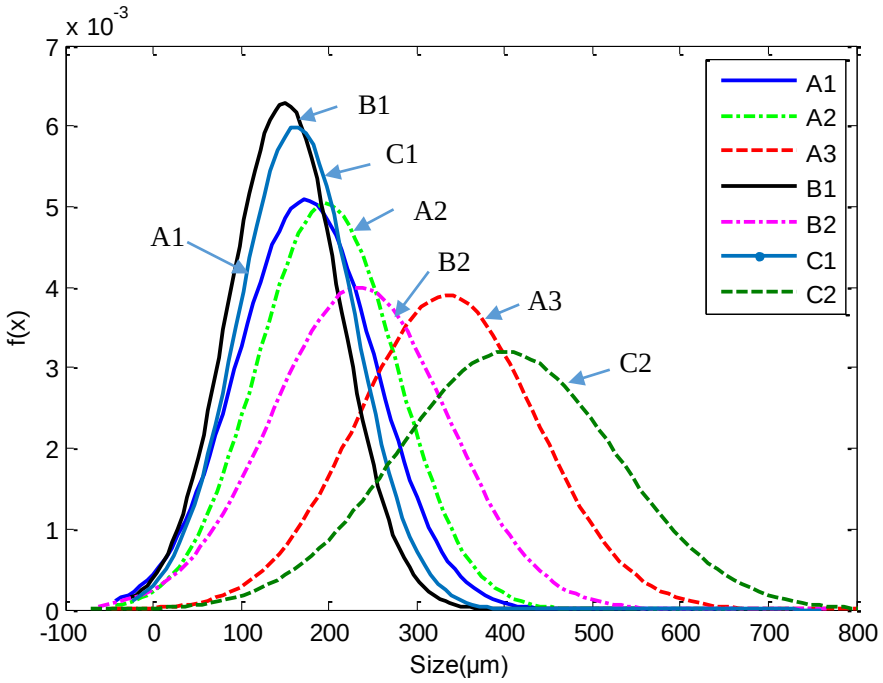

Figure 7. Comparison of crystal size distributions in length under different operating conditions

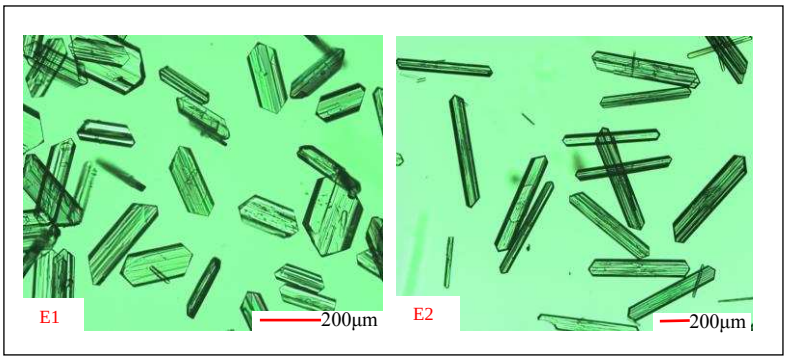

Figure 8. Microscopy images of crystal products by verification experiments